Shear Deformation and Division of Cylindrical Walls in Free-Standing Nematic Films under High Electric Fields

ARTICLE *in* THE JOURNAL OF PHYSICAL CHEMISTRY B · OCTOBER 2008

Impact Factor: 3.3 · DOI: 10.1021/jp806018d · Source: PubMed

2 AUTHORS:

Pramod Tadapatri
Raman Research Institute
9 PUBLICATIONS **76** CITATIONS

SEE PROFILE

K. S. - Krishnamurthy
Centre for Nano and Soft Matter Sciences (…
41 PUBLICATIONS **239** CITATIONS

SEE PROFILE

Shear Deformation and Division of Cylindrical Walls in Free-Standing Nematic Films under High Electric Fields

Pramod Tadapatri and K. S. Krishnamurthy*

Centre for Liquid Crystal Research, P.O. Box 1329, Jalahalli, Bangalore 560013, India

Received: July 8, 2008; Revised Manuscript Received: July 31, 2008

We report on the behavior of cylindrical walls formed in a substrate-free nematic film of PCH5 under the action of an in-plane ac field. In the film, with vertical molecular alignment at all the limiting surfaces, annular Brochard−Leger walls are induced well above the bend−Freedericksz threshold. They exhibit, at high field strengths, a new type of instability not encountered in sandwich, or any other, cell configuration. It manifests as a shearing of the loop-wall between the opposite free-surfaces. The shear strain is measured as a function of time, field strength, frequency, and temperature. Significantly, the strain is linear in field strength. The origin of shear and its dependence on field variables are explained through an adaptation of the Carr−Helfrich mechanism of charge separation. The sheared wall is stable against pincement up to several times the threshold field, and divides itself into two fragments under a large enough strain. With the shear distortion, linear defects appear in the opposite splay-bend regions, just as Neel lines in Bloch walls of magnetic systems. At very low frequencies, flexoelectric influence on distortion is revealed.

Introduction

The Freedericksz effect in nematic liquid crystals is usually studied in the sandwich geometry, employing monodomain samples driven by a suitable external field.[1] It manifests above a threshold constraint as a director-tilt originating in the sample midplane and extending increasingly toward the substrates with field elevation. The orientational states corresponding to positive and negative tilts are degenerate in terms of free energy and occur with equal probability. The transitional zone between two such opposite tilt regions constitutes the so-called Brochard−Leger (BL) wall. In fact, Brochard[2] was the first to carry out a theoretical analysis of the static and dynamic behavior of the walls generated by magnetic fields; from magnetic Freedericksz experiments, Leger[3] verified the main predictions of this analysis. The soliton character of BL walls was revealed in a subsequent theoretical work[4] based on the analogy between nerve-signal propagation and motion of the BL wall.

Electrically generated walls in planarly aligned sandwich samples[5] behave in a more complex way compared to magnetically excited BL walls.[3] For example, in the magnetic case, the wall thickness δ is predicted[2] and observed to be linear in $(\beta^2 - 1)^{-1/2}$, with β denoting the ratio of applied field to the Freedericksz threshold; but δ varies as $(\beta^2 - 1)^{-1}$ in the electric case. Similarly, the equilibrium shape of closed walls, instead of remaining elliptical with the major-to-minor axis ratio determined by the ratio of corresponding elastic constants, turns angular along the major axis in high electric fields. Such deviations are broadly attributed to ionic impurities. In a more recent investigation of electrically excited closed walls in freely suspended films under an in-plane field,[6] several new features not encountered in sandwich geometry came to light. Important among these are (i) shearing of loop-walls revealing discontinuity of the wall along the field direction, in the splay-bend (SB) region, (ii) dependence of the wall-ellipticity on field frequency, and (iii) multiple division of walls under high field strengths. These aspects noted in qualitative terms in a preliminary investigation,[6] are explored quantitatively and discussed in this report. In particular, we argue that the shearing of annular walls is explicable in terms of the Carr−Helfrich (CH) mechanism of charge separation.

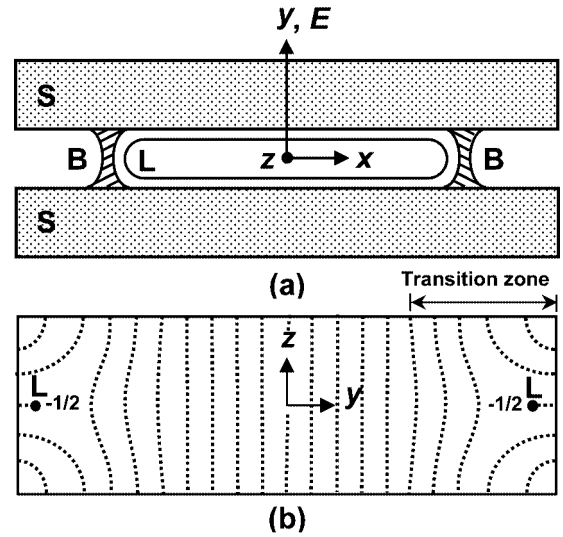

Figure 1. (a) Top-view of sample configuration showing the electrodes S, insulating bridges B, −1/2 disclination loop L, and reference axes (*x*, *y*, *z*); *E* denotes the field. (b) Director field represented by dotted lines, with −1/2 disclination loop in the midplane *xy*. The alignment changes from planar to homeotropic in the transition layer.

Experimental Methods

The nematic liquid crystal used in this study is 4-(*trans*-4′-pentylcyclohexyl) benzonitrile (PCH5) supplied by Merck and having the crystal−nematic temperature T_{KN} of 31 °C and nematic−isotropic temperature T_{NI} of 54.6 °C. Upon cooling, the nematic phase is found to persist in the supercooled state at 25 °C for several hours. The experimental geometry is shown in Figure 1. The electrode strips, made of stainless steel, are

* Corresponding author. E-mail: murthyksk@gmail.com.

10.1021/jp806018d CCC: $40.75
Published on Web 09/23/2008

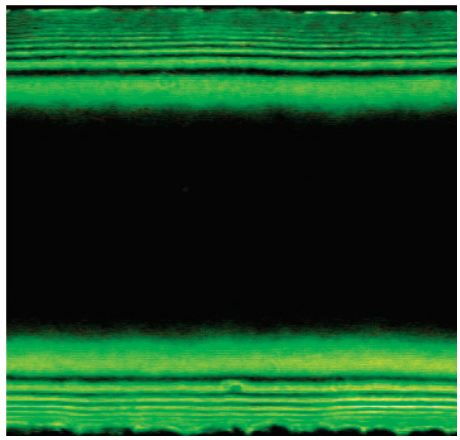

Figure 2. Birefringence fringes near the electrodes in a freestanding film of PCH5 in the field-off state. The central dark region is pseudoisotropic. 40 °C. Sample width $\Gamma = 590\ \mu$m, $d = 175\ \mu$m (d is chosen large to display the transition zone clearly).

held apart by a distance Γ in the range 250−500 μm. The sample thickness d in the central region was estimated from birefringence measurements[7] using a tilt compensator; for this purpose, the alignment of the sample was first made substantially planar by subjecting it to a 100 kHz, 300 V field. The x-dimension of the film was in the range 1−1.5 cm. Observations were carried out in transmitted mercury green light under a Leitz DMRXP polarizing microscope equipped with a Mettler hot stage. Interferograms were all obtained with diagonally oriented polarizers. The images were recorded using a Sony CCD camera. For time series, a FlashPoint 3Dx/4XL frame grabber card was used. The electric field was applied along y. The voltage source was a Stanford Research Systems DS 345 function generator coupled to a FLC Electronics voltage amplifier (model A800). The applied voltage V was measured with an HP 34401A multimeter.

Results

A. Sample Configuration. For a substance such as PCH5 with a large longitudinal molecular dipole moment, the polar coefficient of surface tension is expected to be much greater than the quadrupolar coefficient.[8,9] As a result, at both nematic−air and nematic−solid interfaces, there exists a significant smectic-like order with a strong homeotropic anchoring. Accordingly, in the field-off state, the equilibrium director pattern in a free-standing nematic film of PCH5 is determined by antagonistic boundary conditions that enforce formation of a −1/2 wedge disclination loop L separating the outer SB transition region from the inner homeotropic zone, as shown in Figure 1a. The corresponding director field in the vertical section $x = 0$ and for the case of the loop L lying in the midplane $z = 0$ is depicted in Figure 1b. Usually, the segments of L contiguous to electrode-edges remain pinned to the latter and are not optically resolved; but the curved ends of L appear well separated from the bridges B. Further, in practice, different segments of loop L next to electrode-edges may lie at arbitrary z-positions depending on the substrate conditions, as will be discussed in the next section. Figure 2 presents a typical optical texture of the film in the field-off state, as seen using crossed polarizers set diagonally with respect to x and y. The nature of movement of the horizontal birefringence fringes near the electrodes with rotation of a tilt-compensator confirms the SB nature of distortion in the transition layers.

B. Formation of Linear Walls. The SB transition boundary in the sample plays a significant role with regard to the nature of field-induced distortion. In its absence, assuming a strong homeotropic anchoring at the free surface, the bend−Freedericksz threshold $E_F = V_F/\Gamma$ would be derived[1] by balancing the dielectric torque against the elastic torque as $V_F = (\pi\Gamma/d)(k_{33}/\varepsilon_o\varepsilon_a)^{1/2}$. Here, $\varepsilon_a = (\varepsilon_{||} - \varepsilon_\perp)$ is the dielectric anisotropy, with $\varepsilon_{||}$ and $\varepsilon_\perp$ representing the permittivities along and perpendicular to the nematic director **n**, respectively; ε_o is the permittivity of free space, k_{33} is the bend elastic constant, and Γ is the sample dimension along y. From the reported values of k_{33} and ε_a for PCH5,[7,10] and the aspect ratio $\Gamma/d = 4$ that we used in many of our experiments, we obtain $V_F \approx 5$ V at 30 °C. Thus, the bend−Freedericksz distortion should set in at this voltage in the midplane $z = 0$ for a homeotropic monodomain with no lateral anchoring effects. However, under a quasistatic increase of the field, the dielectric response is found to occur at a much lower critical voltage V_c (∼3 V); it takes the form of an inward expansion of transition layers next to the electrodes, rather than reorientation in the midplane. In fact, the central homeotropic region about $y = 0$ remains unperturbed as long as $[(V_F/V_c) - 1]$ is well below unity. This behavior is to be expected since, within the transition layers, the average molecular orientation at any given y has an initial inlayer component, which conceivably could begin to grow under a field parallel to it at a voltage lower than V_F. The driving force $-dU/dy$ for the transition layer comes from the excess free energy dU in the initial homeotropic state over the energy in the final SB distortion state of the volume corresponding to an incremental advance dy of the layer.[11] Second, even without the orientational transition near the electrodes, because of wetting and meniscus formation at the supporting edges, the increased thickness lowers the threshold.

The transition layers advancing along $\pm y$ in the field-on state are eventually found to either form a BL-like wall stretching along x midway between the electrodes or merge smoothly with each other. The relative symmetry between the director fields in the opposite boundary layers, as illustrated in Figure 3a−d, could explain these mutually exclusive results. For example, in Figure 3a, the line segments of L next to the electrodes are both located below the mid xy-plane with the director field symmetric with respect to the mid yz-plane; thus, under an electric field, growth of the SB regions leads to wall formation, as indicated in Figure 3b. Similarly, in Figure 3c, the segments of L are located on either side of the mid xy-plane, which is favorable to a smooth merger of the advancing transition layers under an applied field, as indicated in Figure 3d. Above a threshold voltage, typically in the range 10−15 V, the SB walls transform into a pair of half-strength disclinations through the pincement process.[12,13] Similar features have been discussed in detail in our earlier reports[6,14] on the field-effects in free-standing nematic films of 4-octyl-4′-cyanobiphenyl (8CB). The focus here is mainly on the effects that are associated with closed walls formed in the high field regime.

C. Formation of Annular Walls. When a field that is about twice the threshold V_F is suddenly applied, simultaneously with a rapid inward motion of the boundary layers, a bend distortion evolves in the central homeotropic region. When the SB curvatures in the leading parts of the transition layers are alike, as in Figure 3c, but opposed to the curvature in the central region, closed walls can form, as depicted in Figure 3e. As pointed out very early by Brochard,[2] the equilibrium geometry of closed walls, obtained through minimization of the cyclic integral of wall-energy per unit length, is an ellipse with the major axis ($2a$) along the field direction being $(k_{11}/k_{22})^{1/2}$ times the minor axis ($2b$), with k_{11} and k_{22} as the splay and twist elastic

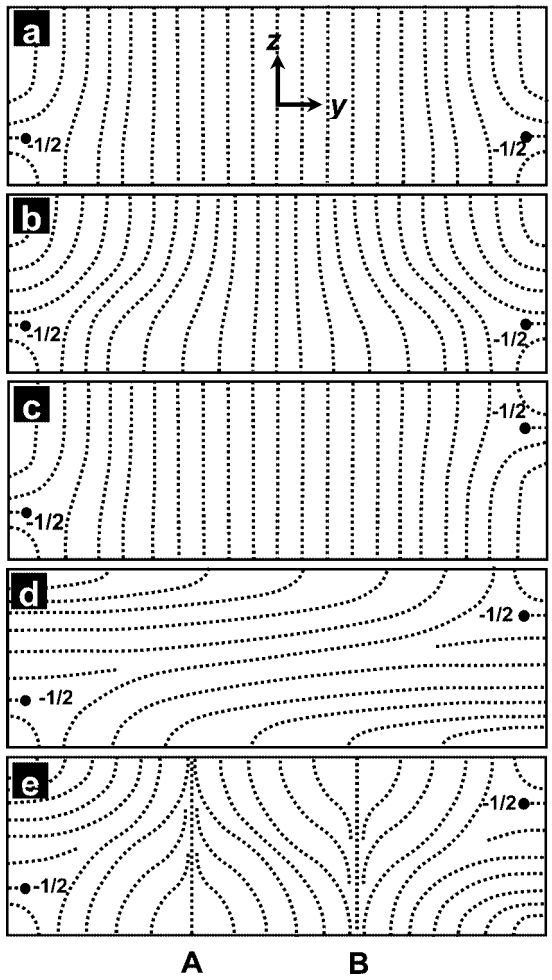

Figure 3. Director configurations. (a) The disclinations located below the mid *xy*-plane with the director field symmetric with respect to the mid *yz*-plane. (b) Growth of the SB regions in panel "a" leading to wall formation under an electric field. (c) The disclinations located on either side of the mid *xy*-plane and unfavorable to wall-formation. (d) Smooth merger of the advancing transition layers in panel "c" under an applied field. (e) Annular wall formed through the Freedericksz perturbation of the director field in panel "c".

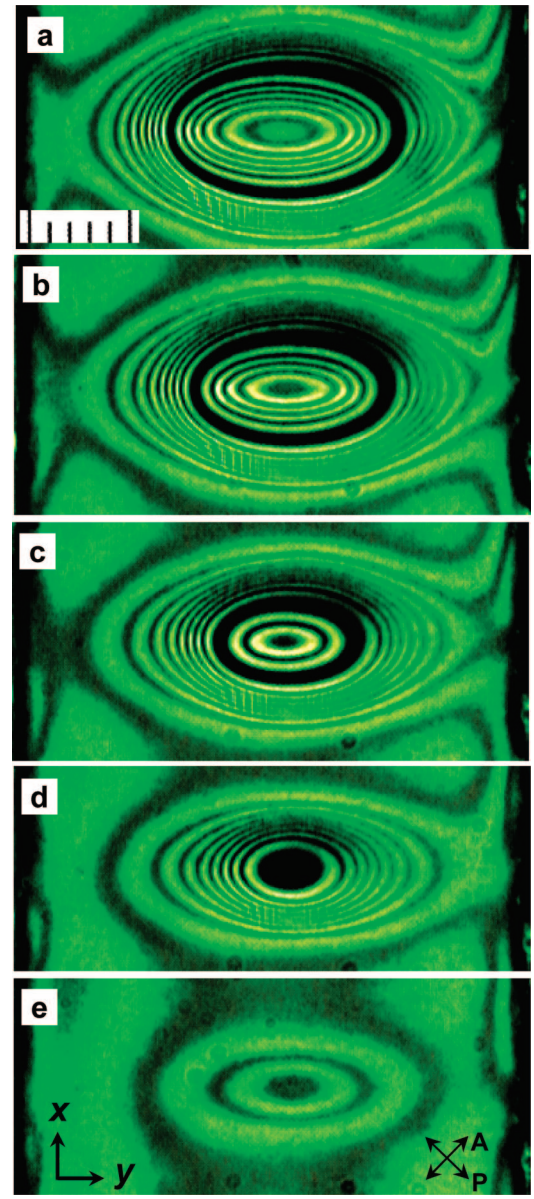

Figure 4. Interferograms of a collapsing wall, with the successive images captured at 1 s intervals. $T = 35$ °C, $d = 80$ μm, $\Gamma = 325$ μm, 150 Hz, 8 V. Scale division 10 μm.

moduli, respectively. Further, closed walls, although irregular in form to begin with, are unstable and, during their spontaneous collapse, assume the equilibrium shape. The rate of collapse $s = da/dt$ along the major axis, obtained by balancing the energy loss due to friction against the energy gain from size-reduction, is $s = k_{11}/(\gamma_1 a)$, where γ_1 is the rotational viscosity.

In Figure 4, we present the interferograms of a closed wall captured during its collapse at an interval of 1 s between successive images. With passage of time, the birefringence fringes move inward and vanish one after another at the center. With the homeotropic core of the wall (at A and B, Figure 3e) approaching the center, the structure of the wall becomes increasingly asymmetric, as the schematic of the director pattern in Figure 5 illustrates. Despite these structural changes, it is interesting that the prediction of the Brochard theory[2] with regard to $s(a)$ largely hold almost up to the point of disappearance of loop walls, as seen in Figure 6. In particular, the collapse rate s scales inversely as the major axis as seen in Figure 6. However, the experimental ellipticity a/b is close to $(k_{33}/k_{22})^{1/2}$ rather than $(k_{11}/k_{22})^{1/2}$; in Figure 4a, it is 1.7, which is quite the same as derived from the elastic constants k_{33} and k_{22};[7,10] further, toward the end, as the loop-dimensions become increasingly smaller than the equilibrium wall-thickness, the ellipticity progressively rises to ~1.9. There exists another significant point of departure from the theory with regard to the magnitude of the rate of collapse. It is predicted that the slope of the s versus a^{-1} line equals the ratio k_{11}/γ_1; but its value of 496 μm^2/s in Figure 6 is ~4.2 times the ratio of k_{11} to γ_1.[10,15]

D. Shearing of Closed Walls. With increase in E, a corresponding decrease occurs in the electric coherence length $\xi \propto 1/E$ along z as well as the wall thickness $\delta \propto 1/[\beta(\beta - 1)^{1/2}]$.[4] For a field ~$4E_F$, when δ is very small compared to its near-threshold value, a remarkable new instability is exhibited by the annular walls in free-standing films, the like of which is not encountered in sandwich geometry. It consists of the shearing of the top and bottom free-surfaces of the domain enclosed by the wall, as schematically represented in Figure 7. Thereby, the opposite sides of the cylindrical wall facing the electrodes become visible under the microscope. Most interestingly, in the SB regions at the extremities of the principal axis along y, structural discontinuities appear (see Figure 10 discussed later). It is the central theme here to characterize and discuss these novel aspects of wall distortion and structure.

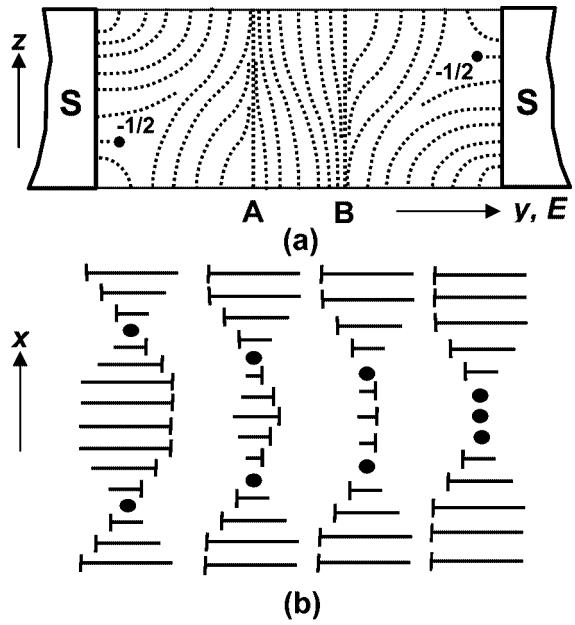

Figure 5. (a) Structural asymmetry in the SB regions of a collapsing loop-wall, dotted lines representing the director field. (b) Progressive change (from left to right) in the twist distortion of a collapsing loop-wall along *x*.

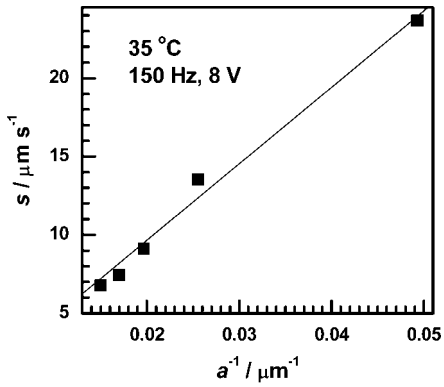

Figure 6. Dependence of the collapse rate *s* of an elliptical wall on its principal dimension 2*a* along the field direction; *s* is linear in 1/*a*.

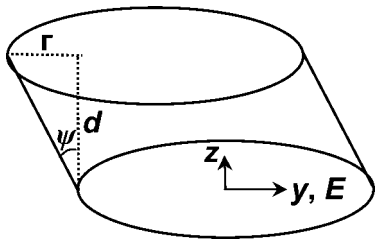

Figure 7. Schematic of the shear distortion in a cylindrical wall. The centers of the domain faces are displaced oppositely through *r* corresponding to a strain tan $\psi = r/d$.

With reference to Figure 7, we may define the shearing strain as tan $\psi = r/d$, *r* being the displacement between the opposite faces. From a study of collapsing closed walls captured in the time series mode, we find that tan ψ is a linearly increasing function of *t* for any given (*V*, *f*). In Figure 8 illustrating this behavior, in order to adopt a uniform time scale, the end point of the collapse process has been taken as the reference time $t = 0$. From the slopes of the lines here, it is evident that the time rate of increase of strain $(\tan \psi)'$ is strongly dependent on the applied field (Figure 9). To exemplify the voltage dependence of strain at a given frequency, we consider the tan ψ values obtained from the wall images recorded at $t \approx -2$ s, and corresponding very nearly to the maximum strain developed at each of the voltages. In the interferograms in Figure 10 recorded at various voltages, with $f = 25$ Hz and $t \approx -2$ s, a systematic increase in the strain with *V* is evident. That this increase is linear is demonstrated in Figure 11 giving the data for different frequencies. Further, from the slopes of the lines here, a decrease in the degree of shear with increase in *f* is inferable; shear strain, as shown in Figure 12, is a quadratic function of *f*. In consonance with these results, upon suddenly switching over from a low *f* (<50 Hz) to a relatively high *f* (>200 Hz) at a fixed voltage, the shear is seen to totally disappear, as in Figure 13.

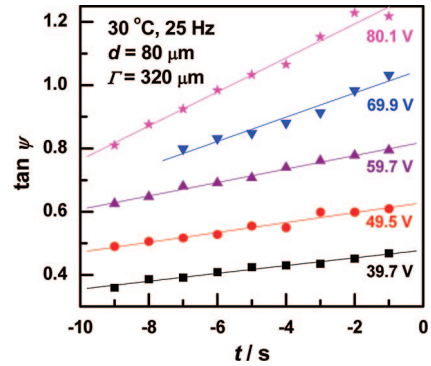

Figure 8. Time variation of shear strain at various voltages.

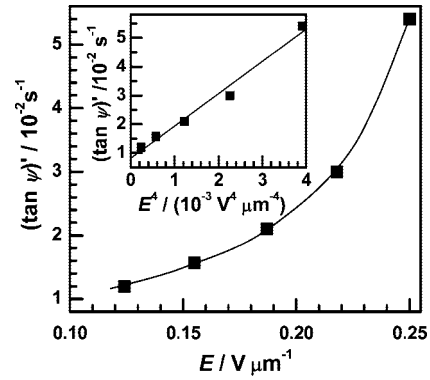

Figure 9. Rate of increase in the shear strain as a function of the applied field from the data in Figure 8. The inset shows linearity of the rate of shear strain in E^4.

Figure 14 shows the temperature dependence of shear. The data involve a considerable scatter and, within experimental error, ln(tan ψ) may be considered to be linear in (1/*T*); this is in consonance with an exponential decrease of viscosity with rising temperature.

At low frequencies and high voltages, as for example at 20 Hz and 100 V, the shear becomes so large that the wall, in the course of its collapse and continued shearing, develops a "neck" that becomes ever narrower with efflux of time, and eventually divides into two. Further divisions of each of the fragments are also observed at very high voltages. Various walls formed under identical conditions and displaying different stages of fission are presented in Figure 15.

At very low frequencies ($f < 2$ Hz), in the opposite SB regions of the wall, the degree of distortion shows a subtle difference that becomes conspicuous in a square wave field, as demonstrated in Figure 16. Here, between the successive images, the field direction alternates. A difference between the fringe-patterns formed at the wall-extremities along *y* is evident in all

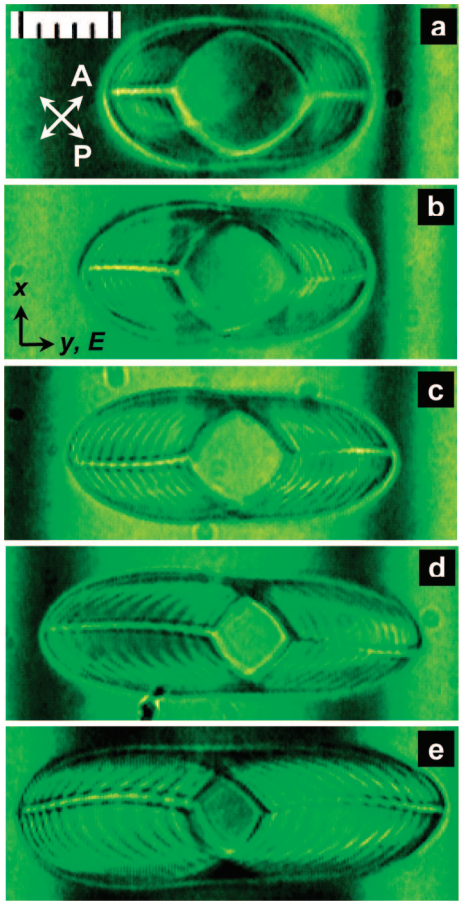

Figure 10. Interferograms of collapsing closed walls at various voltages captured ~2 s prior to their complete disappearance. Voltages: (a) 40 V, (b) 50 V, (c) 60 V, (d) 70 V, (e) 80 V. $T = 30$ °C, $d = 79.5$ μm, $\Gamma = 325$ μm. Scale division 10 μm.

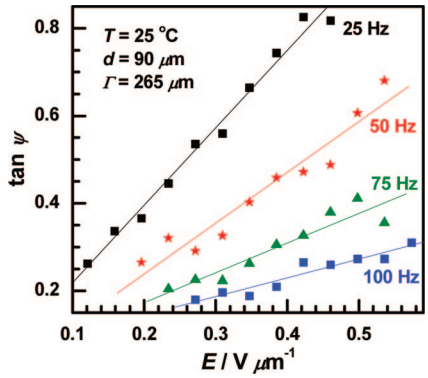

Figure 11. Dependence of shear strain on field strength at various frequencies.

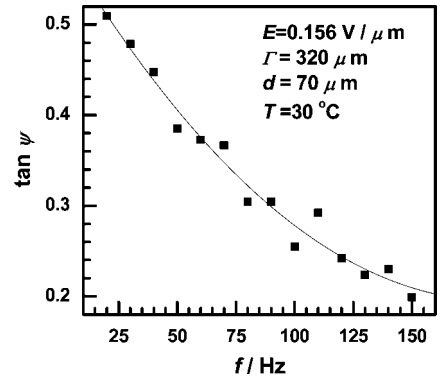

Figure 12. Frequency variation of shear strain.

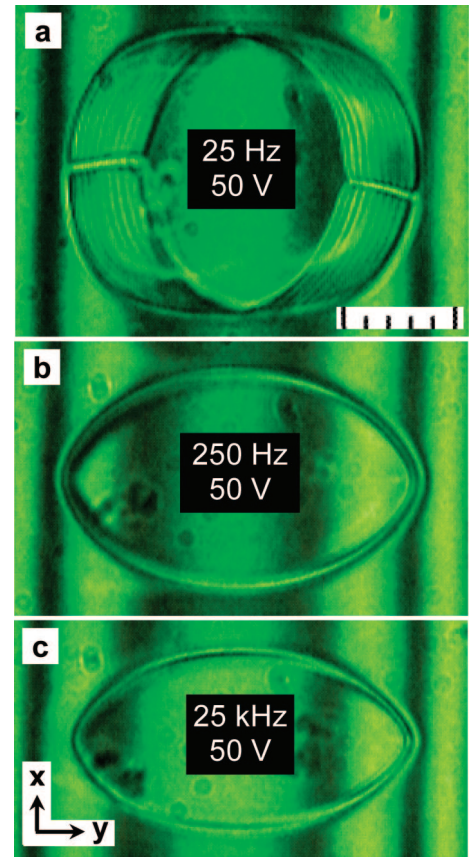

Figure 13. Effects on shear distortion and wall-geometry produced by sudden changes in frequency at constant voltage. (a) Interferogram of a wall with pronounced shear strain and nearly circular cross section. (b) Same wall as in panel "a", immediately after switching f to 250 Hz, displaying a nearly elliptical cross-section and practically no shear. (c) Image of the wall on a further switching of f showing slightly increased ellipticity. $T = 30$ °C, $d = 75$ μm, $\Gamma = 325$ μm. Scale division 10 μm.

the images. In panels a and c, the line defect is better defined in the upper part indicating a stronger distortion there compared to the lower part. The reverse is true in panels b and d. The asymmetry of distortion is thus related to the field direction.

For voltages several times the threshold V_F, when the shearing takes place, the theoretical results derived for an insulating nematic cannot be expected to hold good. Nevertheless, for ease of later discussion, we may mention a result concerning the time dependence of the principal axes D_x and D_y of closed walls. The ratio (D_y/D_x), as shown in Figure 17, is a smooth quadratic function of time, and we have verified this for voltages in the range 40−100 V. When $D_x > D_y$ to begin with, (D_y/D_x) increases continuously through its equilibrium value (~1.7 at 35 °C) to over 2.5 near collapse point. The product D_yD_x, which is a measure of the cross-sectional area, is a linearly decreasing function of time. This feature, interestingly, is in accordance with the Brochard theory, despite the varying behavior of (D_y/D_x), since the predicted constancy of both $a(da/dt)$ and a/b implies a steady rate of decrease of the loop area.

Discussion

In freely suspended nematic films, as pointed out early by Faetti et al.,[16] two very different electric field generated effects are possible, and it is necessary for us to consider each of them

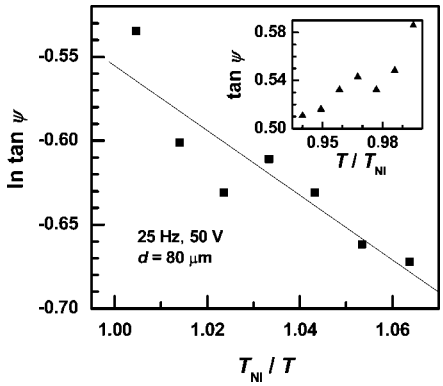

Figure 14. Temperature dependence of shear strain; tan ψ is nearly exponential in (T_{NI}/T) within experimental error. The inset shows the variation of tan ψ with (T/T_{NI}).

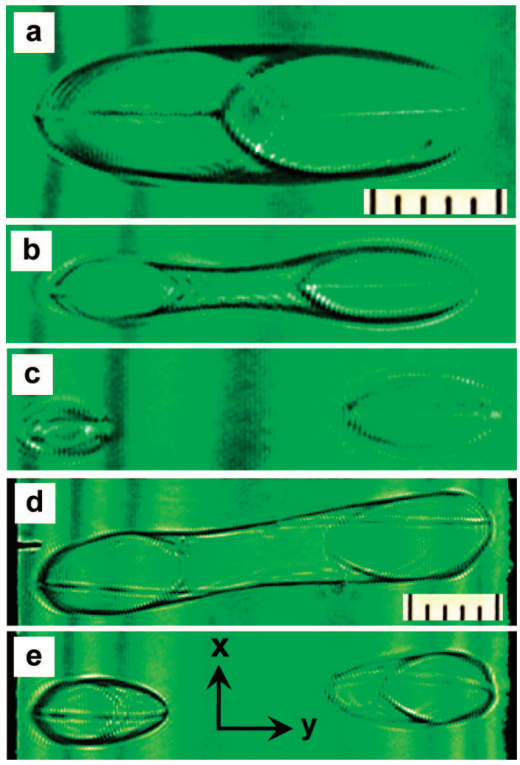

Figure 15. Division of loop-walls under increasing shear strain and decreasing domain-size, with passage of time. 20 Hz, 24.1 °C. 112 V (a−c), 150 V (d,e). The images are of different walls in various stages of division. Scale division 10 μm.

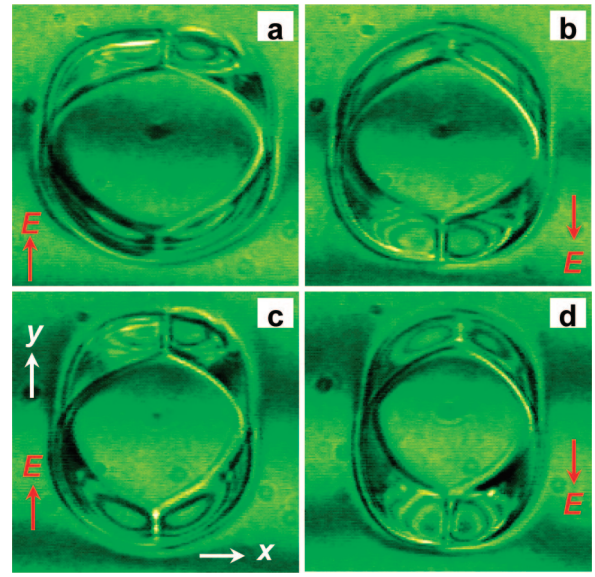

Figure 16. Effect of field reversal on distortion as observed under very low frequency, square-wave excitation. Arrows in red show the field direction. $T = 30$ °C, $d = 113$ μm, $\Gamma = 435$ μm. 0.2 Hz, 40 V.

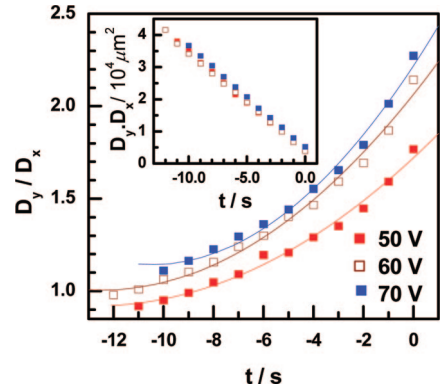

Figure 17. Time variation of the ellipticity of closed walls at different voltage amplitudes. The continuous curves are second order polynomial fits. The inset shows the linear time dependence of the cross-sectional area of loop domains.

in attempting to understand the origin of the shearing phenomenon. First, we have the interaction between surface charges and the applied field.[16a] In practice, nematics contain ionic species and act as weak electrolytes. Electric charges accumulate at the free surfaces near the electrodes because of the discontinuity in electrical conductivity, σ. In equilibrium, the space charge density is such that the normal component of the field at the interface vanishes within the film. The positive and negative surface charges existing near the electrodes of like polarity are, below a threshold voltage V_V, uniformly distributed along x with a decreasing density along y; above V_V, the surface charge density becomes periodic in x such that fluid breaks up into an array of vortices along x, with the adjacent vortices having opposite angular momentum, and the sense of rotation reversing with field polarity. This vortex mode (VM) is an isotropic electrohydrodynamic effect not dependent on the anisotropic material parameters and found in nematic and isotropic liquids[16] as well as smectics.[17] We did not observe the VM instability in PCH5 for the reason that V_V, which scales as d both in theory and experiment, is expected to be in the range of a few kilovolts for a 100 μm thick sample such as used here.[16a] Further, to produce the electrical shear stress, we need the free surfaces of the loop domains to carry opposite charges; but, selective accumulation of space charges on the domain faces due to the isotropic mechanism of the VM is difficult to envisage. However, the surface charges near the electrodes could affect the dynamics of shear.

The second important effect is that driven by the well-known CH mechanism,[18] which is based primarily on the anisotropy of electrical conductivity $\sigma_a = (\sigma_{||} - \sigma_{\perp})$, where || and $\perp$ refer to the directions relative to the nematic director, **n**. Originally, it was invoked to explain electroconvection (EC) in nematics having a negative ε_a and positive σ_a, and planarly aligned in sandwich cells; the CH analysis of the coupling between σ_a and the bend curvature distortion leads to periodic space charges of alternating sign appearing along the alignment direction, x. The body force on these charges sets up periodic cellular flows above a critical voltage V_t determined by the balance between hydrodynamic, dielectric, and elastic torques. An extension of

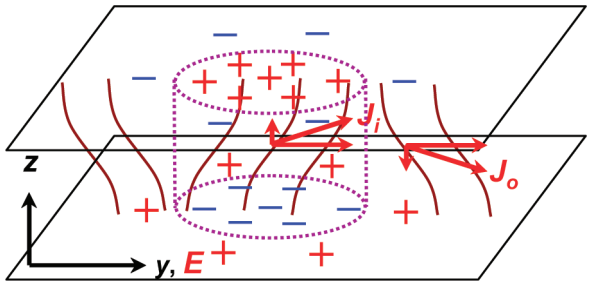

Figure 18. Schematic of the model of charge separation through the CH mechanism. $\boldsymbol{J}_i$ and $\boldsymbol{J}_o$ are respectively the current densities inside and outside the domain enclosed by the BL wall for a field E along y.

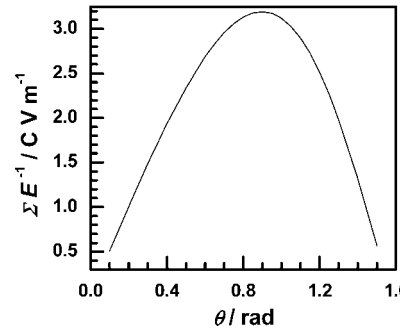

Figure 19. Theoretical space charge density for unit field strength as a function of the director tilt angle for PCH5 at 35 °C according to ref 17.

this model to freely suspended homeotropic nematic films subject to an in-plane field[16b] leads to a patterned state with the onset voltage:

$$V_t = \left[\frac{\pi^2(k_{33}+k_{22}s)(\sigma_{\parallel}+\sigma_{\perp}s)}{(1+s)\left(\varepsilon_a\sigma_{\perp}-\dfrac{\alpha_2(\varepsilon_{\perp}\sigma_{\parallel}-\sigma_{\perp}\varepsilon_{\parallel})}{\eta_3+\eta_2 s}\right)}\right]^{1/2}(\Gamma/d),$$

$$\text{with } s=\frac{k^2\Gamma^2}{\pi^2}, \text{ and } k=\frac{2\pi}{\lambda}\sim\frac{1}{\Gamma}$$

Here, k is the pattern wavenumber and λ, the wavelength; α_2, η_2, and η_3 are appropriate viscosity parameters. For PCH5, mainly because of the large value of ε_a, the denominator within the braces becomes negative and no real solution emerges for V_t (see refs 7, 15, and 19 for the data required to arrive at V_t). This does not, however, rule out charge separation arising from the anisotropy in σ. In fact, as indicated in Figure 18, the CH mechanism could not only be active, but also lead to the shearing of loop walls. For the tilt of the molecules within the loop-wall as in the figure, given σ_a to be positive, the current density $\boldsymbol{J}_i$ due to a steady field along y, will be at an angle to the field in the yz-plane; it will have an upward component leading to positive space charges at the upper face and negative charges at the lower one. The reverse is the case outside the wall. For reasons of symmetry, neither of the two faces of the loop wall is subject to any net electrical force due to the surrounding charges generated by the CH process. The force of the applied field on these faces will act oppositely so that a shear strain is produced. Under an ac field, since the sign of the charges on the domain faces interchange with every polarity reversal, the shearing sense remains unaffected. In the domain mode (DM) model, Faetti et al.[16b] suppose a periodic variation along x of the polar angle θ of **n** confined to the yz-plane; then the opposite average tilts in the adjacent domains lead to a periodic charge density variation along x, with charges of opposite sign recurring alternately. In PCH5, the dielectric torque is so strong that a periodic twist deformation is not sustained.

Keeping in view the foregoing model of charge accumulation, we may now examine qualitatively the significance of our results. The space charges $\pm q(t)$ developed over the domain faces are, in equilibrium, expected to decrease in proportion to the decrease in the area A of the faces. As long as the shear stress qE/A is unchanged, the shearing strain tan ψ may remain constant in time. Experimentally, $A(t)$ is linearly decreasing (Figure 17) while tan $\psi(t)$ is linearly increasing (Figure 8). By implication, the space charges do not diffuse across the wall in any observable measure as the wall collapses. When the mean molecular tilt inside the loop domain is a decreasing function of time (Figure 5), the charge density could in fact increase with collapse in the regime of large tilts, as we shall discuss presently, and this could explain the effective constancy of q.

The linear, rather than quadratic, dependence of the strain on E (Figure 11) may seem more intriguing at first sight. If the space charge density $q/A = \Sigma$ were to scale as E, we would expect the shear stress to scale as E^2. However, Σ also involves the director tilt with respect to the field direction, θ. The steady state value of Σ, determined by the requirement that the net transverse current is stopped by the space charge field, is given by[18]

$$\Sigma=\frac{(\sigma_{\parallel}\varepsilon_{\perp}-\varepsilon_{\parallel}\sigma_{\perp})\cos\theta\sin\theta}{(\sigma_{\parallel}\cos^2\theta+\sigma_{\perp}\sin^2\theta)}E \qquad (1)$$

In classical EC experiments using planarly aligned (−, +), that is, negative ε_a and positive σ_a, nematics in sandwich geometry, the field-off state is dielectrically stable, and the field-induced director tilt begins to saturate[20] at angle $\theta_s = \tan^{-1}(\sigma_{\parallel}/\sigma_{\perp})^{1/2}$. In the geometry used here, and with large ε_a, θ approaches 90° at very high voltages. Thus, the shearing situation corresponds to a large tilt angle. From Figure 19 based on eq (1), we see that, in the high-tilt region, Σ/E decreases almost linearly as θ increases. It is thus quite conceivable, the changes in E and its coefficient in eq (1) are mutually compensating, so that Σ does not vary significantly with E. In that case, the shear stress $\Pi = \Sigma E$ and the strain tan ψ could vary essentially as E.

The observed influence of frequency on the degree of shear (Figures 12 and 13) is in accordance with the CH-mechanism-based space charge build-up which depends on the charge relaxation time, $\tau = \varepsilon_o\,\varepsilon_{\perp}/\sigma_{\perp}$, and becomes progressively less effective as f increases. At 35 °C, for example, for PCH5, τ = 5.94 ms. Above a field frequency of about τ^{-1} the charges cannot follow the field, and expectedly, therefore, the shear is absent in Figure 13b.

The distortion asymmetry seen in the images of Figure 16 is an effect likely to be linear in field unlike the Freedericksz effect, which is quadratic. We may associate it with flexoelectric polarization $\boldsymbol{P}_f$ developed in the opposite SB regions (at A and B in Figure 3e). The directions of $\boldsymbol{P}_f$ in the two regions are related through inversion symmetry, being up−down in the absence of shear; with shear, $\boldsymbol{P}_f$ acquires an in-plane component $\boldsymbol{P}_{fy}$ that is directed oppositely in the two regions. Since a net $\boldsymbol{P}_{fy}$ lowers the free energy, it is reasonable to suppose the SB distortion to become stronger where the polarization is along E, and weaker where it is opposite.

The division of a closed domain, such as seen in Figure 15, is a phenomenon quite different from the bursting of a liquid drop suspended in another immiscible liquid under a large electric stress.[21] In the latter case, the deformation and division

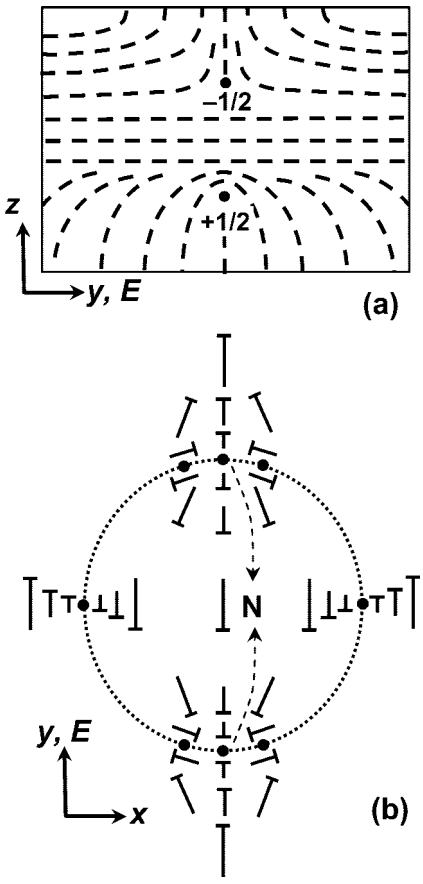

Figure 20. (a) Schematic director-field representation to show the transformation of a BL wall into a pair of half-strength singular lines of opposite topological charge. (b) Structure of the loop-wall under high field strengths indicating the formation of Neel-like lines at N with oppositely twisted regions on either side.

are not due to anisotropic conduction, but to the discontinuous change of the electrical properties at the interface; for leaky dielectric fluids with $\varepsilon_d/\sigma_d \neq \varepsilon_s/\sigma_s$, d and s referring to the drop and surrounding fluid, respectively, the result is an accumulation of opposite charges on the hemispheres facing the electrodes; these charges contribute to the deformation of the drop into oblate or prolate form, and cause circulations in both the fluids; burst is, in general, a consequence of the inability of the capillary pressures in the deformed drop to balance the electric and hydrodynamic stresses at the interface. Some of these considerations have also been applied to cylindrical nematic (isotropic) domains surrounded by an isotropic (a nematic) fluid and the deformation is observed to be proportional to the square of the field strength, as in the case of spherical drops.[22] In the case of cylindrical domains here, the field dependence of shear deformation is linear and we do not observe any electrohydrodynamic streaming even at low frequencies. The division of collapsing domains is a result of elastic and viscous torques failing to balance the electrical shear torque. Moreover, the cylindrical wall is not a sharp boundary, and the enclosed volume is time dependent.

Open BL walls terminating at the boundaries become unstable when the field reaches $\sim 2E_F$ and undergo pincement or decomposition into a pair of disclinations (Figure 20a).[12−14] Pincement is sometimes induced even in cylindrical walls on their coming into contact with some form of discontinuity such as a foreign particle or an electrode-edge, and the three-dimensional (3-D) nature of closed walls becomes quite evident in this process; one of the resulting disclinations, very likely the +1/2 line, appears as a collapsing loop, and the other attaches itself at the boundary (see Figure D of the Supporting Information). Interestingly, the sheared loop walls away from the boundaries exhibit a remarkable stability against pincement or decomposition into a pair of disclinations (Figure 20a) even when E/E_F reaches 20 or more. On the other hand, shear is associated with a different type of line defects that extend across the film thickness in the opposite SB regions of sheared walls (see, for example, Figure 10). Their origin may be understood in terms of elastic free energy, which, considering $k_{11}/k_{22} \sim 1.6$ and $k_{33}/k_{22} \sim 3$, is quite large for splay-bend deformation relative to that for twist. Thus the SB deformation, in high fields, tends to relax in favor of a less energetic, although more complex, structure that is mostly twist. The corresponding director field, schematically represented in Figure 20b, is reminiscent of the changed SB structure of an Ising wall in a high magnetic field.[12,23] Since the twist has to match with the opposite chiralities at the extremities of the principal axis along *x*, its sense reverses upon crossing the symmetry plane *yz*. The oppositely twisted regions get connected through a twist line-defect of unit strength, just as a Neel line between reverse Bloch walls in magnetic systems (shown at N in Figure 20b).[24]

Conclusions

Cylindrical BL walls in free-standing nematic films behave very differently from similar walls in sandwich geometry. They are remarkably stable against decomposition into singular lines in very high fields, but develop a complex shearing instability leading to a division of the loop-domain. We have invoked the CH mechanism of anisotropic-conduction-induced charge separation to explain in qualitative terms the origin of shear and its dependence on time, field strength, and frequency. Many factors that could influence the degree of shear and its time variation have been ignored. For example, the free surfaces are treated as planar while, at the solid boundary, menisci are actually formed.[25] Similarly, space charges at free surfaces near the electrodes, injection of charge carriers at low frequencies and surface polarization due to dipole alignments at bounding surfaces are some of the other factors. Despite these limitations, there seems to be little doubt that the primary cause of the shearing phenomenon is the ion segregation via the CH process.

Acknowledgment. We thank Professor K. A. Suresh for his support and encouragement. K.S.K. is thankful to the Department of Science and Technology, India, for the Indo-Bulgarian research project under which this work is conducted. We are indebted to M/s Merck Limited for supplying PCH5 free of charge.

Supporting Information Available: A word file providing details of birefringence fringes in sheared annular walls, director patterns for walls undergoing division, and decomposition of closed walls into singular lines. This information is available free of charge via the Internet at http://pubs.acs.org.

References and Notes

(1) Blinov, L. M.; Chigrinov, V. G. *Electrooptic Effects in Liquid Crystal Materials*; Springer: Berlin, 1994.
(2) Brochard, F. *J. Phys. (Paris)* **1972**, *33*, 607.
(3) Leger, L. *Mol. Cryst. Liq. Cryst.* **1973**, *24*, 33.
(4) Wang, X. Y *Phys. Lett.* **1985**, *112A*, 402. Here the thickness of the BL wall is predicted to vary inversely as $\beta(\beta-1)^{1/2}$ with $\beta = E/E_F$.
(5) Krishnamurthy, K. S.; Bhate, M. S. *Mol. Cryst.Liq. Cryst.* **1985**, *128*, 29.

(6) Krishnamurthy, K. S.; Balakrishnan, R. *Pramana* **2003**, *61*, 263.

(7) Pohl, L.; Finkenzeller, U. In *Liquid Crystals: Applications and Uses*; Bahadur, B., Ed.; World Scientific: Singapore, 1990; Vol. 1, pp 139−170. The extraordinary and ordinary refractive indices, n_e and n_o, for 589 nm, are $n_e = 1.5845$ and $n_o = 1.4794$ at 30 °C and $n_e = 1.5807$ and $n_o = 1.4785$ at 35 °C.

(8) Parsons, J. D. *Phys. Rev. Lett.* **1978**, *41*, 877.

(9) Sonin, A. A.; Yethiraj, A.; Bechhoefer, J.; Frisken, B. *Phys. Rev. E* **1995**, *52*, 6260.

(10) From ref 7, at 30 °C, $k_{11} = 8.2$ pN, $k_{22} = 5.1$ pN, $k_{33} = 15.6$ pN, and $\varepsilon_a = 11.4$. At 35 °C, $k_{11} = 7.5$ pN, $k_{22} = 4.8$ pN, $k_{33} = 13.8$ pN, and $\varepsilon_a = 10.9$.

(11) Cladis, P. E.; van Saarloos, W.; Finn, P. L.; Kortan, A. R *Phys. Rev. Lett.* **1987**, *58*, 222. This report concerns the field-induced motion of disclination lines occurring at high field strengths rather than the growth of SB boundaries in the absence of any perceptible motion of disclination lines observed here at lower fields. In both cases, in view of the considerable *x*-dimension of samples, end effects are ignored, and disclinations/transition layers parallel to the electrodes are considered.

(12) de Lozar, A.; Schopf, W.; Rehberg, I.; Svensek, D.; Kramer, L. *Phys. Rev. E* **2005**, *72*, 051713.

(13) Vella, A.; Intartaglia, R.; Blanc, C.; Smalyukh, I. I.; Lavrentovich, O. D.; Nobili, M. *Phys. Rev. E* **2005**, *71*, 061705.

(14) Krishnamurthy, K. S.; Balakrishnan, R. *Liq. Cryst.* **2002**, *29*, 383.

(15) Eich, A.; Wolf, B. A.; Bennett, L.; Hess, S *J. Chem. Phys.* **2000**, *113*, 3829. $\gamma_1 = 0.061$ Pa s.

(16) (a) Faetti, S.; Fronzoni, L.; Rolla, P. A. *J. Chem. Phys.* **1983**, *79*, 5054. (b) Faetti, S.; Fronzoni, L.; Rolla, P. A. *J. Chem. Phys.* **1983**, *79*, 1427.

(17) Daya, Z. A.; Morris, S. W. *Phys. Rev. E* **1997**, *55*, 2682, and references therein.

(18) Helfrich, W. *J. Chem. Phys.* **1969**, *51*, 4092.

(19) For PCH5 at 35 °C: From ref 15, in Pa s, $\eta_1 = 0.075$, $\eta_2 = 0.011$, $\gamma_1 = (\alpha_3 - \alpha_2) = 0.061$, and $\gamma_2 = (\alpha_3 + \alpha_2) = -0.0644$; $\eta_3 = (0.6\eta_1\eta_2)^{1/2}$ from the empirical scaling behavior of the Miesowicz coefficients discussed in Simoes, M.; Domiciano, S. M.; Alves, F. S. *Liq. Cryst.* **2006**, *33*, 849; thus, $\eta_3 = 0.022$ Pa s; from ref 8, $\varepsilon_{\parallel} = 16.0$, $\varepsilon_{\perp} = 5.1$; from our measurements, $\sigma_{\parallel} = 11.92$ nS m^{-1}, $\sigma_{\perp} = 7.60$ nS m^{-1}.

(20) Carroll, T. O. *J. Appl. Phys.* **1972**, *43*, 1342.

(21) Torza, S.; Cox, R. G.; Mason, S. G. *Phil. Trans. R. Soc. London* **1971**, *A269*, 295.

(22) Park, C. S.; Clark, N. A.; Noble, R. D. *Phys. Rev. Lett.* **1994**, *72*, 1838.

(23) Chevallard, C.; Nobili, M.; Gilli, J.-M. *Liq. Cryst.* **2001**, *28*, 179.

(24) Kleman, M. *Points, Lines, and Walls in Liquid Crystals, Magnetic Systems, and Various Ordered Media*; John Wiley & Sons: New York, 1983.

(25) The thickness *d* is generally uniform in the central zone extending over a distance of ∼Γ/3 along *y*; on either side, *d* increases nonlinearly. In a typical case, we found for a sample with $\Gamma = 385$ μm, $d \approx 76$ μm over a width of 135 μm, and $d \approx 90$ μm near the electrode-edges.

JP806018D